

Graphene oxide coated PU 다공성 소재를 활용한 AAV 플랫폼용

3D printing 열가소성 흡음 복합재 구조

3D printed sound-absorbing thermoplastic folded core sandwich structure based on porous materials and microperforations

Abstract

본 연구에서는 Graphene oxide coated PU 다공성 소재를 활용한 AAV 플랫폼용 3D printing 열가소성 흡음 복합재 구조를 제안하였다. 제안된 샌드위치 구조는 단탄소섬유가 분산된 Polyamide(CF-PA)와 연속탄소섬유(CCF) 필라멘트, 그래핀 옥사이드가 코팅된 폴리우레탄 폼으로 구성되었다. 면재는 CCF와 CF-PA를 각각 강화재, 기지재로 하여 물성을 적용하였고, 코어는 CF-PA 물성값만을 적용하여 설계하였다. 시뮬레이션 결과, 코어와 미세 천공의 최적화된 매개변수가 저주파수 (160-1600 Hz)대역에서 흡음 성능을 향상시키는 것을 확인하였다. 또한, 다공성 소재인 그래핀 옥사이드가 코팅된 폴리우레탄 폼을 삽입하여 중·고주파수 대역 (1600-6000 Hz)에서 흡음 성능 및 기계적 물성이 향상됨을 확인하였다.

Key Words : Thermoplastic, 3D printing, Folded core sandwich composites, Micro-perforated panel, Sound absorption coefficients, AAV (Advanced air vehicle)

1. Introduction

Advances in industrial development and transportation have significantly increased noise pollution, and the advent of advanced air vehicle (AAV) has contributed to this problem. The transportation of cargo and low altitude travel by AAV cause a disturbance in the soundscape, leading to adverse effects on industry and the human body^(1~4). As a result, interest in sound absorption and suppression has increased. Sound absorption is the process by which the sound energy propagating through a material is reduced by absorption and transmission when it reaches the surface of the material. Consequently, there are two primary methods of sound absorption: absorption through the use of sound absorption materials (SAMs) and the implementation of sound absorption structures (SASs). SAM is the most commonly used sound absorption technology, using porous materials such as polyurethane (PU) foam and polyester. However, SAM is inefficient in absorbing sound from low-frequency bands, which is a drawback of this method^(5~11). To improve the sound absorption performance in the low-frequency band, active research has been conducted on SAS, a sound absorption method at the structural level. Compared with SAMs, SASs offer the advantages of superior mechanical properties and lightweight construction, making them a promising alternative⁽¹²⁾. Recent studies have focused on investigating SAS in the context of structures with periodic patterns, artificial porous structures using microperforated panels (MPPs), and sandwich structures to improve their sound absorption properties^(13~16). These MPPs are structures with air cavities usually smaller than one millimeter. Studies have been conducted to improve the sound absorption coefficient (SAC) by applying MPPs to general face sheets of sandwich structures^(17~23).

Three-dimensional (3D) printing, also known as additive manufacturing (AM), has the advantage of producing complex 3D structures that are simpler than the existing composite manufacturing process^(24~30). They are classified into different types depending on the material and process^(31~33), including fused deposition modeling (FDM), stereolithography (SLA), and selective laser sintering (SLS). FDM is a popular and simple process in which a filament of thermoplastic polymer is melted and extruded using a nozzle heated above the glass transition temperature, and

the material is deposited one at a time to create the final object⁽³⁴⁾. The filaments used in FDM 3D printing are usually plastic, such as polylactic acid (PLA), acrylonitrile butadiene styrene (ABS), and polyamide (PA), which have relatively poor mechanical properties. Currently, researchers are exploring methods to improve the mechanical properties of 3D-printed objects by incorporating continuous carbon fiber (CCF) filaments into the manufacturing process⁽³⁵⁻⁴⁵⁾. CCF has better specific stiffness and strength than aluminum and steel, and therefore can significantly contribute to weight reduction, which is a core technology in aviation, and technological development is ongoing⁽⁴⁶⁻⁵⁰⁾. As mentioned earlier, fabrication is relatively simple because complex geometric designs are converted to G-code. Consequently, interconnections between the parts are reduced, allowing the integration of parts thanks to mass production. In addition, the number of fasteners, such as nuts and bolts, has been reduced, so weight reduction is more effective. In addition, manufacturing costs can be reduced and the production processes can be automated. Meng et al⁽⁵¹⁾. developed a sandwich structure with a corrugated core and a microperforated panel (MPP). They then measured the sound absorption coefficient (SAC) for different design variables, including the diameters and densities of the microperforations in the face sheet and core. The researchers then proposed a sandwich structure with outstanding sound absorption performance by comparing and analyzing the measured SAC values and the analytical solution obtained by acoustic analysis. Using FDM fabrication, the researchers produced both the face sheet and the core and found that the micro-perforated structure had a sound absorption performance of over 99 % within a specific frequency band (100-1000 Hz). In addition, they found that increasing the diameter of the microperforations resulted in a higher peak value for the SAC. Chao et al⁽⁵²⁾. presented a sandwich structure with superior mechanical properties achieved by fabricating a honeycomb core sandwich structure using FDM and incorporating CCF to compensate for the poor mechanical properties of 3D printing. The researchers found that compared to a honeycomb structure made of pure PLA, the addition of CCF increased the mass of the structure by 6%. However, compressive stiffness and energy absorption, were also significantly improved, by 86.3 % and 100 %, respectively. Akiwate et al⁽⁵³⁾. conducted a study to investigate the effect of the design parameters of the honeycomb core and the size and shape of the microperforations, on the sound absorption performance over a wide frequency range (0-6000 Hz). To this end, they fabricated an acrylonitrile butadiene styrene (ABS) face sheet and core and conducted experiments. They found that a shorter honeycomb cell length improved sound absorption at higher frequencies, whereas triangular microperforations gave the best acoustic performance. The researchers also found that the highest SAC value exceeded 98 % when the diameter of the microperforation was 1.09 mm (in the range of 1.09-2.33 mm). Alternatively, Oh et al⁽⁵⁴⁾. assessed the sound absorption and impact energy absorption of a PU foam coated with flake-shaped graphene oxide (GO). The researchers found that the GO-coated PU foam had significantly better sound absorption properties than the uncoated foam, with a 99.7 % sound absorption coefficient at 2236 Hz. In addition, the absorption of impact energy was 189 % higher for the GO-coated foam than for the uncoated foam. These results confirmed that the porous structure of the GO-coated PU foam effectively absorbed both sound and impact. Table 1 summarizes the reports on sandwich structures, confirming the mechanical properties and SAC of 3D printed microperforations, with diameters ranging from 0.6 to 2.33 mm^(51, 53, 55-60). Based on the design parameters, the SACs were measured in the low-, mid-, and high-frequency bands using the impedance tube method. The mechanical properties were verified by compression tests. However, the 3D printed structures described above were limited to plastic filaments, resulting in insufficient mechanical strength because only polymer matrix composites were used. Therefore, it is important to develop thermoplastic composite structures with a combination of porous materials to improve the sound absorption and mechanical properties of multifunctional composite structures.

Table 1.

Literature reports on the sound-absorbing performance and mechanical properties of 3D printing composites along with microperforations.

No.	3D printing conditions		Core types	Sound absorption conditions		Mechanical properties
	Printing methods	Materials		Frequency [Hz]	Perforations diameter [mm]	Compression load [N]
Current study	FDM	Continuous carbon fiber, Chopped carbon fiber-PA	Folded core	150–1600	1	830
[31]	FDM	-	Corrugated core	100–1600	1	-
[35]	-	-	Face-centered cubic core	100–1600	1	-
[33]	FDM	ABS	Honeycomb core	800–6300	1.09–2.33	-
[36]	SLA	VisiJet - SL	-	500–5500	0.6	-
[37]	FDM	PLA	Lattice core	-	-	650
[38]	SLA	Ceramic	Diamond core, Honeycomb core	-	-	423, 160
[39]	FDM	PLA, PET, TPU	Nitrile, butadiene rubber – PU foam	-	-	480
[40]	FDM	ABS	Folded core	-	-	899

In this study, a folded-core sound-absorbing sandwich composite structure was fabricated using FDM 3D printing method. The fabricated structure contained the CF-PA and CCF filaments, microperforations, and GO-coated PU foam, as shown in Fig. 1. Microperforations in the structure are small apertures that facilitate the dissipation of sound wave energy by causing vibrations in the incident sound waves. At the same time, the V-patterned folded core structure causes multiple scattering of the trapped sound waves, resulting in improved sound absorption performance. However, in the study, a PU foam, which is known for its excellent performance in this frequency range, was used to improve the sound absorption performance at higher frequencies. The PU foam was also coated with a GO dip coating. Graphene oxide exhibits the unique property of converting sound energy into heat energy when sound waves impinge on it in the low-frequency band. The sound absorption performance of the structure was evaluated using the impedance tube method in both the low- and high-frequency bands (160–6000 Hz). In addition, a flatwise compression test was performed to assess the mechanical strength of the sandwich structure filled with the GO-coated PU foam. The results obtained from the simulations and experiments are in good agreement, indicating that the multifunctional composite structure is a candidate for various applications.

In this study, a folded-core sound-absorbing sandwich composite structure was fabricated using FDM 3D printing method. The fabricated structure contained the CF-PA and CCF filaments, microperforations, and GO-coated PU foam, as shown in Fig. 1. Microperforations in the structure are small apertures that facilitate the dissipation of sound wave energy by causing vibrations in the incident sound waves. At the same time, the V-patterned folded core structure causes multiple scattering of the trapped sound waves, resulting in improved sound absorption performance. However, in the study, a PU foam, which is known for its excellent performance in this frequency range, was used to improve the sound absorption performance at higher frequencies. The PU foam was also coated with a GO dip coating. Graphene oxide exhibits the unique property of converting sound energy into heat energy when sound waves impinge on it in the low-frequency band. The sound absorption performance of the structure was evaluated using the impedance tube method in both the low- and high-frequency bands (160–6000 Hz). In addition, a flatwise compression test was performed to assess the mechanical strength of the sandwich structure filled with the GO-coated PU foam. The results obtained from the simulations and experiments are in good agreement, indicating that the multifunctional composite structure is a candidate for various applications.

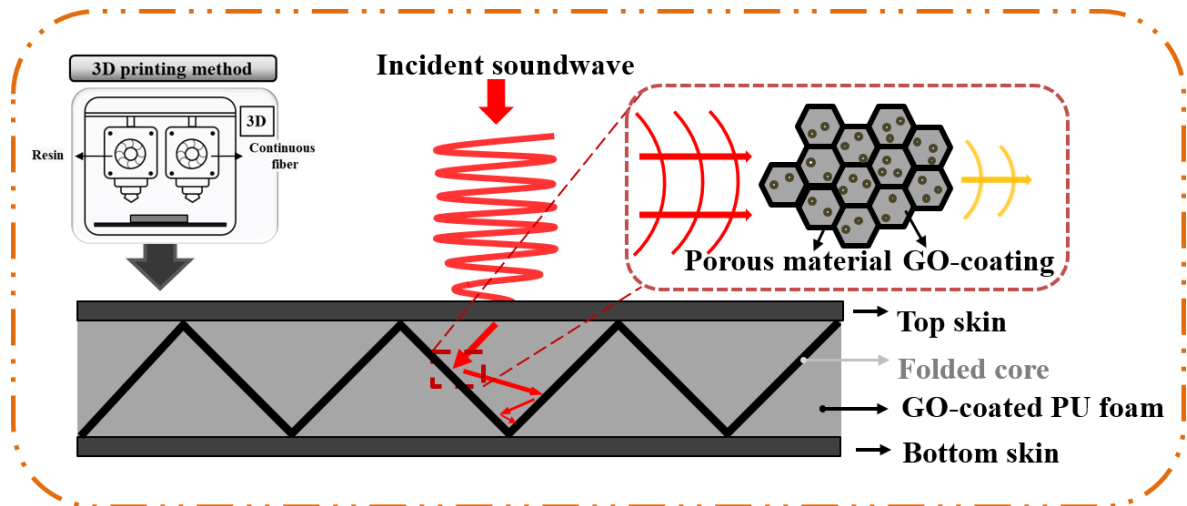


Figure. 1. The schematic diagram of a sound-absorbing folded core sandwich structure with microperforated face sheet

2. Materials and methods

2.1 Materials preparation

In this study, PA filament, which is a thermoplastic polymer commonly used in 3D printing, was selected as the resin. We used Smooth PA filament from Anisoprint, which contains 10.0 wt% chopped carbon fibers. This filament was selected because it has lower water absorption than conventional filaments, which can cause print quality degradation. Water absorption is a chronic problem in 3D printing. By using a filament with a lower water absorption rate, we were able to improve the mechanical strength of the printed object. Fig. 2(a) shows the scanning electron microscopy (SEM; MIRA 3LM, TESCAN, Czech Republic) images of the carbon-fiber-dispersed thermoplastic polyamide (CF-PA) filament. The diameter of the polymer filament was 1.75 mm, and the chopped carbon fibers were dispersed inside the PA filament. Conventional 3D printing methods often rely on the addition of fiber-reinforced composite materials to thermoplastic polymer filaments to improve their mechanical properties. However, in this study, a different approach was taken and Anisoprint's 0.35 mm-diameter CCF filament was used⁽⁴¹⁾. Fig. 2(b) shows SEM images of the CCF filament-printed specimen and a cross-section of the continuous fiber filament. The SEM images show that the fiber bundles were uniformly distributed over the continuous fiber filament and remained stacked even after extrusion through the nozzle.

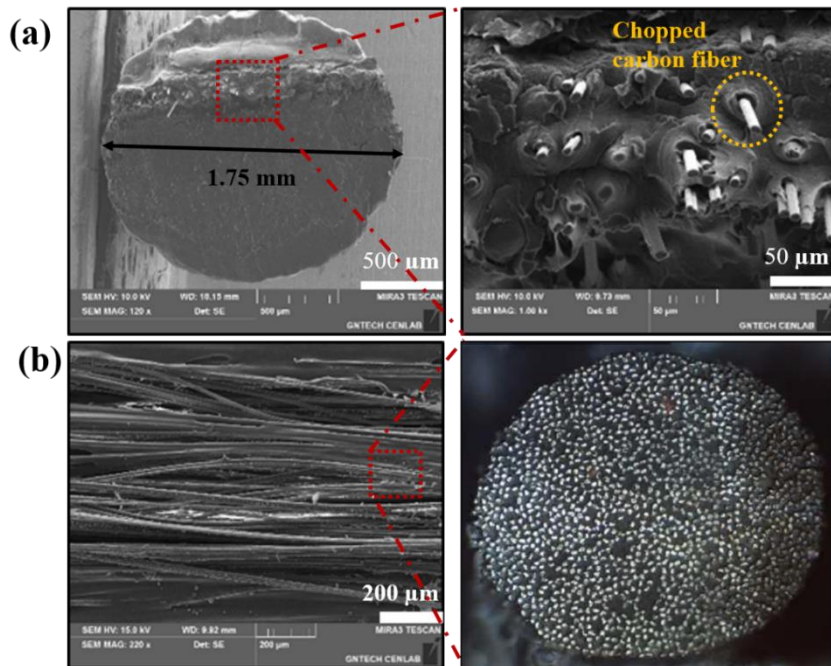


Figure 2. (a) SEM images of CF-PA and (b) CCF filament

A folded-core sandwich structure was developed to improve the low-frequency band acoustic performance with SAS. Meanwhile, sound-absorbing materials, such as PU foam and GO-coated PU foam, were used in the mid- and high-frequency bands. In general, PU foam has excellent sound absorption performance in the high-frequency band but poor sound absorption in the low-frequency region. Accordingly, this study aimed to improve the sound absorption performance in the low-frequency region by GO coating. GO is carbon-based, has high corrosion resistance and conductivity, and is flake-shaped. Therefore, when a sound wave in the low-frequency band is incident, it vibrates microscopically and converts sound energy into friction-heat energy, improving the sound absorption performance in the low-frequency band. In this study, GO was dip-coated onto PU foam. After filling the PU foam with an aqueous GO solution with the composition shown in Table 2, the natural drying process was repeated three to four times to coat the PU foam with GO. The SEM images showed the porous structure of PU and the uniform distribution of GO on the PU foam, as shown in Fig. 3(a,b).

Table 2. The nominal composition of graphene oxide

Nominal composition (wt. %)				
C	O	H	Size [μm]	Thickness [μm]
80	15	5	37–162	2.0–2.4

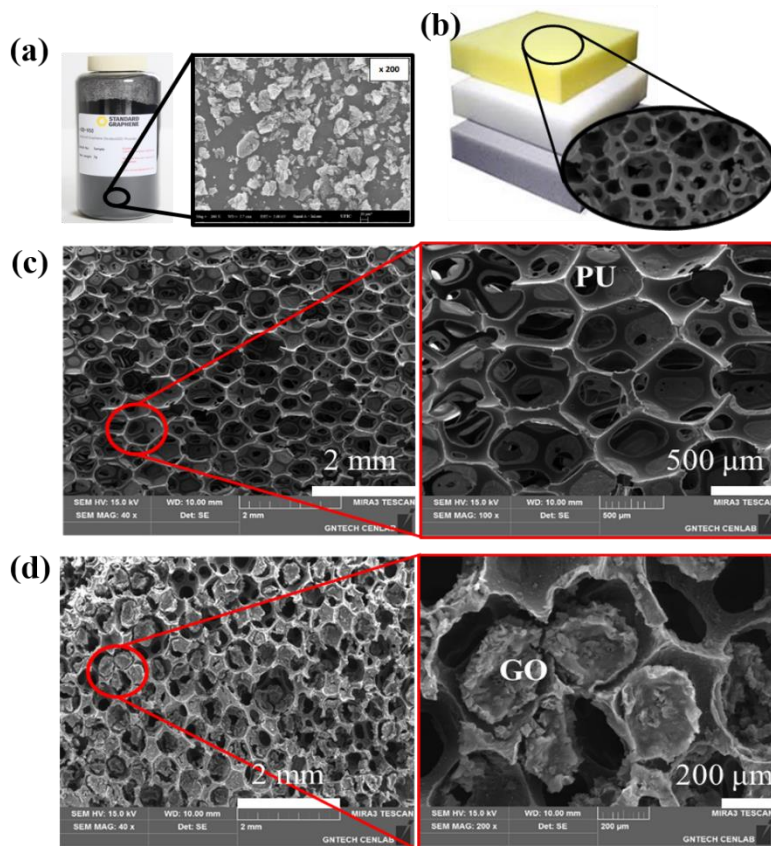


Figure 3. The images of (a) GO solution and (b) pristine PU, the SEM image of (c) pristine PU foam, and (d) GO-coated PU foam

2.2 Methods

A 3D dual-nozzle FDM-type printer (Composer A4, Anisoprint) is used. In the FDM process, a solid thermoplastic polymer filament is passed through a nozzle that is heated above the glass transition temperature, and the molten resin is deposited layer by layer. In addition, FDM-type 3D printers are popular because they are relatively simple to set up and program compared to SLA- and SLS-type printers, and because they can handle a variety of materials. Because it is a method in which raw materials are melted and deposited on a printing bed to cure, one drawback is that separation of layers can occur at the interface. This problem can be overcome by adjusting the output precision and printing parameters. Fig. 4 shows the dual-nozzle printer and the nozzle used in this study. The printer can produce composites as large as 297 × 210 × 140 mm, and when the nozzle temperature increases to 270 °C, various thermoplastic polymer filaments can be applied. In particular, it can be used to extrude thermoplastic polymers and continuous fiber filaments. Prior to the acoustic analysis, the Young’s modulus, Poisson’s ratio, and density were determined for acoustic-structural analysis to confirm the material properties of the thermoplastic polymer composite structure in which the CCF and chopped carbon fibers were dispersed. The tensile tests were performed according to the ASTM D 3039 standard, and the specimens were prepared with dimensions of 250 × 15 × 2 mm. Fig. 5 shows the fabrication process and the test setup. The results are shown in Table 3, together with the results of CF-PA from previous reports^(61,62).

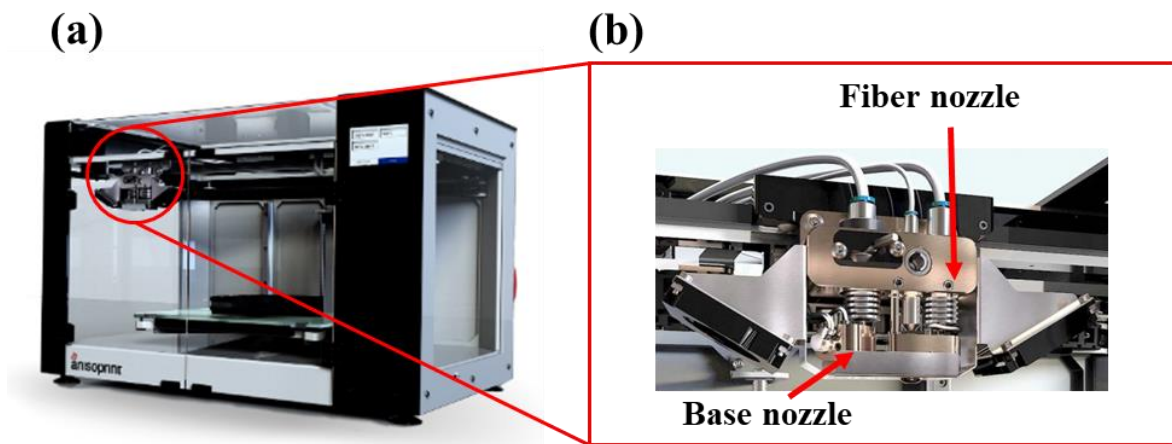


Figure. 4. (a) FDM-type 3D printer (A4) and (b) enlarged view of dual nozzle

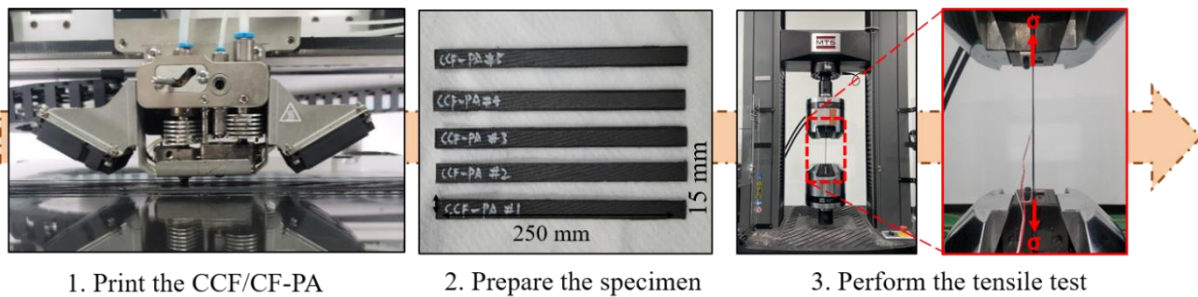


Figure. 5. (a-c) The 3D printing process of CCF/CF-PA tensile specimens and the tensile test setup

Table 3.

Material properties of continuous carbon fiber (CCF)–carbon fiber–dispersed polyamide (CF-PA) and CF-PA.

	CCF/CF-PA	CF-PA
Young's modulus [GPa]	15	3.59 ^[42]
Poisson's ratio	0.42	0.4 ^[43]
Density [kg/m ³]	920 ± 10	930 ± 3

3. Design and fabrication

3.1 The principle of sound-absorbing structure

Sound absorption is the reduction of sound energy when sound passes through a material and is either absorbed or transmitted. The basic principle of sound absorption is that sound waves cause vibrations in structures or porous materials, resulting in compression, expansion, and the reduction of sound energy through thermal and viscous friction. When sound waves encounter voids in these materials, their energy is converted to heat, causing the sound to be absorbed. The Helmholtz equation is a mathematical model for calculating the sound absorption based on a wave equation that describes the change in sound pressure over time and the speed of sound (c). This equation allows the prediction of sound absorption coefficients and can be used to optimize the design of sound-absorbing materials and structures. Fig. 6 illustrates the sound absorption mechanism as determined through the impedance tube method, with the calculation formula shown in (1). This method assumes that the sound energy is not dissipated until it reaches the point of incidence⁽⁵¹⁾.

$$\nabla^2 P = \frac{1}{c^2} \frac{\delta^2 P}{\delta t^2} \quad (1)$$

Sound energy can be divided into three main components: reflection, transmission, and absorption. This relationship can be expressed mathematically using (2)

$$E = E_{ref} + E_{trans} + E_{absorb} \quad (2)$$

The total sound energy can be expressed by (3), and the reflected and transmitted energies are calculated using Eqs. (4) and (5), respectively:

$$E = \frac{1}{2} \int_S P_{in} \cdot V_{in} dS \quad (3)$$

$$E_{ref} = \frac{1}{2} \int_S (P_{total} - P_{in}) \cdot (-V_{total} + V_{in}) dS \quad (4)$$

$$E_{trans} = \frac{1}{2} \int_S P_{trans} \cdot V_{trans} dS \tag{5}$$

SAC (a) can be derived by substituting the reflected and transmitted energies calculated using the above equations into (6).

$$\alpha = 1 - \frac{E_{trans}}{E} - \frac{E_{ref}}{E} \tag{6}$$

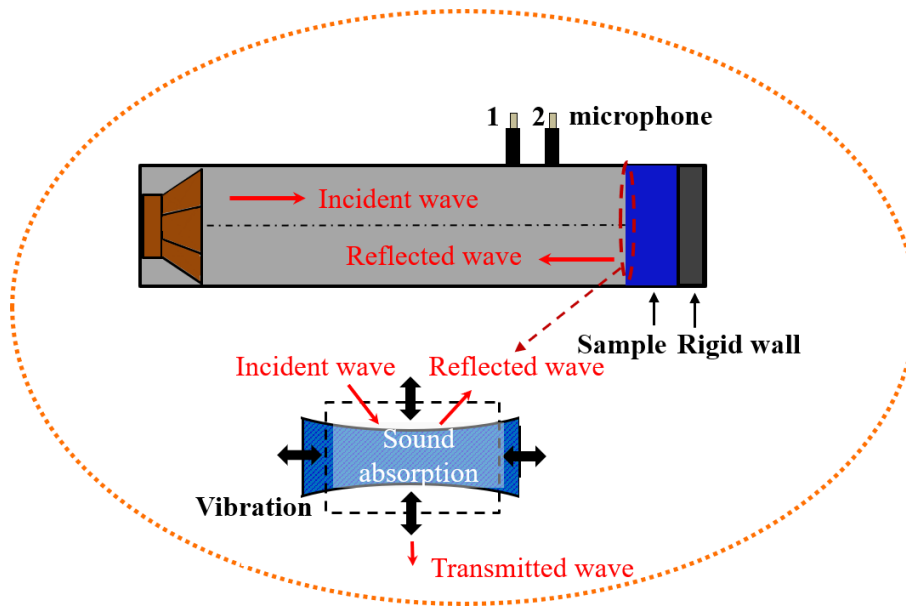


Figure. 6. The schematic diagram of the impedance tube method and the sound absorption mechanism

3.2 Design

A folded core is a 3D structure formed by folding a flat base material, forming a flat surface at a specific angle. This angled surface confines the incident waves within the structure, resulting in repeated multiple scattering and improved sound absorption performance. Structures with microperforations are known to form artificial porous structures that allow for increased airflow and greater structural vibration when incident sound waves are present. This leads to improved sound absorption performance, as the increased vibration and air flow help dissipate the energy of the sound waves. The unit cell of the folded-core sandwich structure is defined by five important configuration variables, including two angles and two lengths, that determine the V-pattern shape, as well as the thickness of the core. These variables are shown in Fig. 7(a). Because the folded core is a sandwich structure, there are other variables that can affect the sound absorption performance. In addition to the five configuration variables for the unit cell, the thicknesses of the upper and lower face sheets and the diameters of the microperforations also play an important role in determining the overall sound absorption efficiency of the structure. To design the folded-core sandwich structure, COMSOL Multiphysics, a commercial software package that enables multiphysics simulations and modeling, was used in this study. Specifically, a unit cell-shaped structure was modeled for the low-frequency band (160–1600 Hz), and an acoustic-structural analysis was performed using the tensile test properties determined in Section 2.2. The resulting material properties are summarized in Table 4 and were used to optimize the design parameters for maximum sound absorption performance in the target frequency range. To construct the folded-core sandwich structure, the material

properties of the CF-PA determined in Section 2.2 were used and applied to the folded core. Both CCF and CF-PA were used for the face sheets of the sandwich structure. It is worth noting that CCF was only applied to the face sheets because its continuous filament structure made it difficult to incorporate into the complex 3D geometry of the folded core. The unit shape of the folded-core sandwich structure, based on the material properties obtained in the previous section, is shown in Fig. 7(b). To evaluate the sound absorption performance of the design, a parametric analysis on the folded core sandwich SAS was performed using various design variables. The names and ranges of the design variables used in the analysis are listed in Table 4.

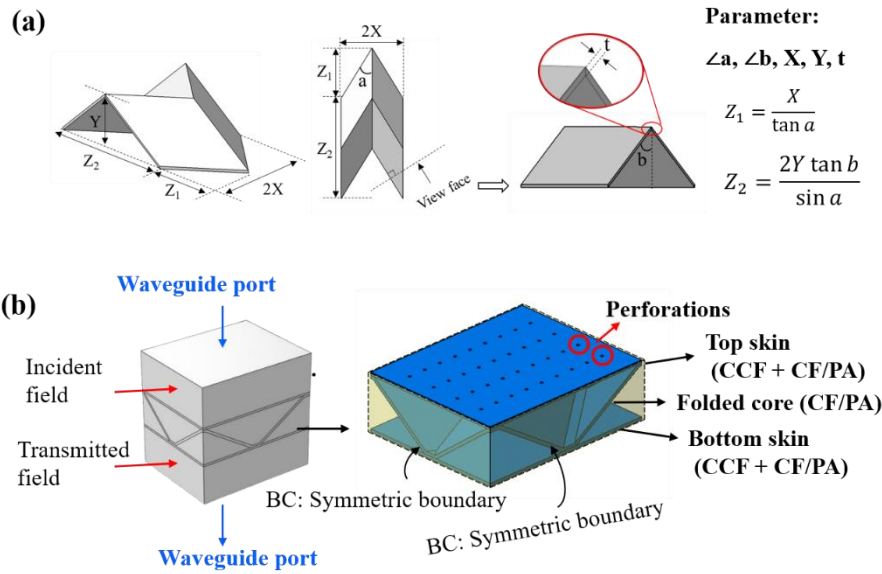


Figure. 7. The (a) parameters of a unit-cell folded core and the (b) simulation model of the unit-cell of the proposed folded core structure

Table 4.

Design parameters of the proposed sound-absorbing folded core sandwich structures.

Structures [materials]	Parameters	Design range [unit]
Folded core [CF-PA]	Dihedral fold angle ($\angle a$)	40–60 [degree]
	Acute angle ($\angle b$)	25–45 [degree]
	Half of the width (X)	10–30 [mm]
	Height (Y)	10–30 [mm]
	Core thickness (t_{core})	0.8–1.4 [mm]
Skin [CCF/CF-PA]	Face sheets thickness (t_{face})	0.8–1.4 [mm]
	Pores' diameters (D)	0.5–1.0 [mm]

To measure the sound absorption performance of the folded-core shape in the low-frequency band using the impedance tube method, a parametric analysis was performed of the half-width (X) and height (Y), which are key determinants of size. Fig. 8(a) shows that there were no significant variance in the sound absorption performance when the half-width was altered. However, based on the results obtained, we decided to set the half-width at 20 mm because the sound absorption performance at this width showed an increasing-to-decreasing trend. As can be seen in Fig. 8(b), the sound absorption performance improved with increasing height, and the peak sound absorption performance shifted to the low-frequency band. Therefore, the height was fixed at 30 mm. Figs. 8(c) and 8(d) illustrate the effects of variations in design parameters, particularly angles "a" and "b" – on sound absorption performance in different frequency domains, as shown. Decreasing the angle "a" caused the peak value of SAC to shift toward the low-frequency band, indicating the best sound absorption performance. In contrast, increasing the angle "b" caused the peak value of SAC to move towards the low-frequency band, showing the best sound absorption performance. It is believed that when the angle "a" decreases and the angle "b" increases, the folded core adopts a more easily vibrating shape, which can improve the sound absorption performance. Consequently, we selected 40° for angle "a" and 45° for angle "b" because they have the best sound absorption performance. Second, a parametric analysis was performed on the thickness of the folded core. Fig. 8(e) shows that the SAC peak value improves with increasing thickness. Nevertheless, because of the 3D printing production time increases significantly as the folded core thickness increases, we decided to use a thickness of 1 mm. We also performed a parametric analysis on the thickness of the sandwich face sheet. As shown in Fig. 8(f), a thinner face sheet resulted in a better SAC peak value. Nevertheless, we selected a thickness of 1 mm because the face sheet cannot accommodate the insertion of CCFs during 3D printing if the thickness is 0.6 or 0.8 mm. Finally, we performed a parametric analysis of the microperforation diameters on the face sheet. Our literature search revealed that an extremely small diameter does not significantly affect the sound absorption performance; therefore, the diameter was set at 0.5 and 1 mm. Our analysis showed that a perforation rate of 1.32 % and a diameter of 1 mm resulted in a sound absorption performance of 99 % or more at 1250 Hz, as shown in Fig. 8(g). Therefore, a microperforation diameter of 1 mm was selected. It was observed that the SAC peak value shifted towards a higher frequency band when the face sheet had microperforations. This shift was attributed to an increase in the air-hole interface area and acoustic resistance, which ultimately increased the resonant frequency and caused the SAC peak value to move from the low-frequency band to a higher-frequency band. Fig. 9 shows the target zones selected based on the results of the parametric design analysis. Fig. 9(a) shows the range of design variables for half width and height, while Fig. 9(b) illustrates the range of angles 'a' and 'b' that define the V-patterned shape of the folded core. Finally, Fig. 9(c) shows the shape parameters defined by the thicknesses of the core and face sheets. Each target zone represents the area with the highest sound absorption performance. To facilitate 3D printing and CCF insertion, the core and face sheet thicknesses in the selected zone were set to 1 mm. Fig. 9(c) shows a visual representation of the design choice.

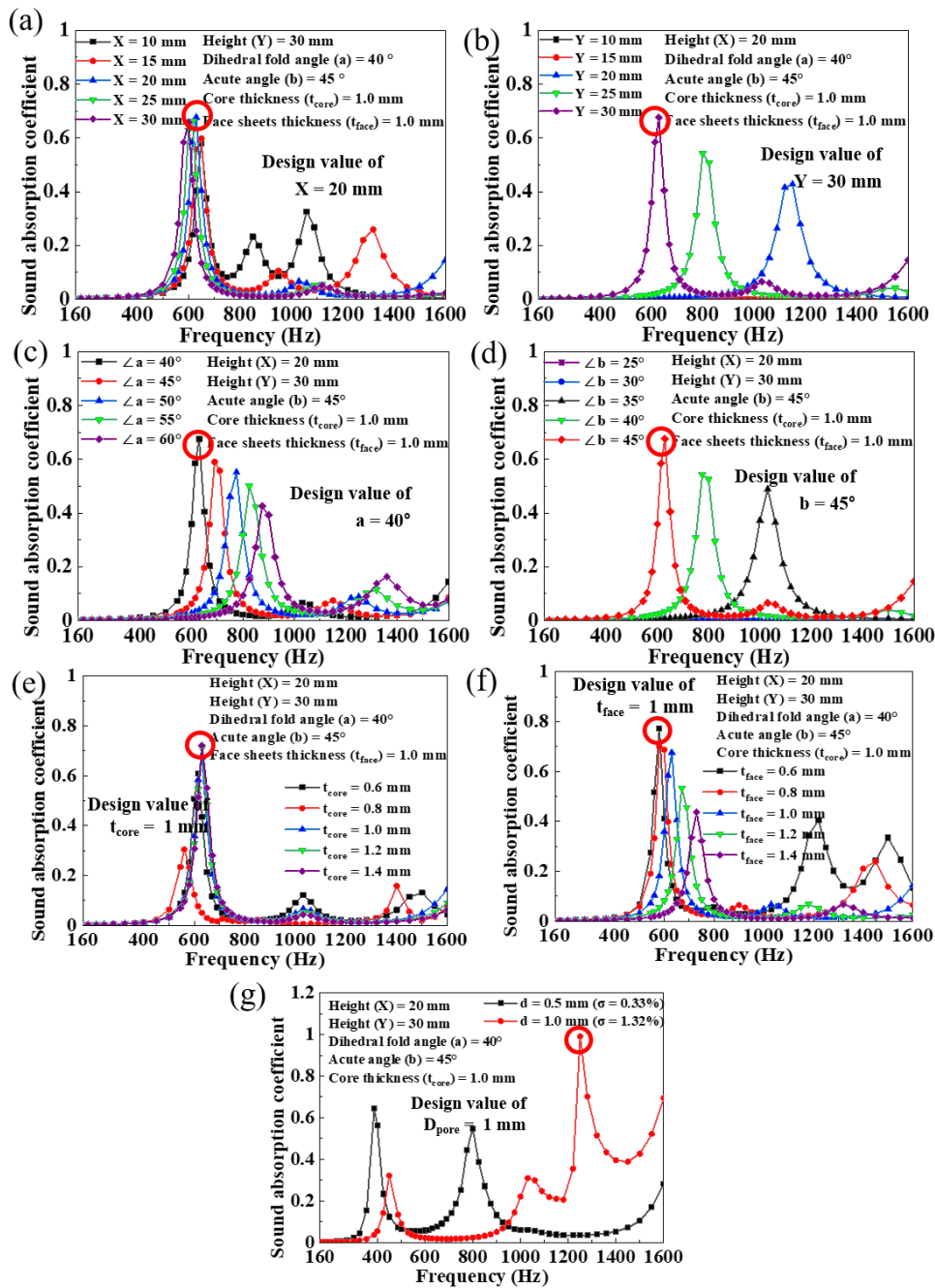


Figure. 8. The effect of variation in design parameters on the sound absorption performance: (a) half of width [X], (b) height [Y], (c) dihedral fold angle [“a”], (d) acute angle [“b”], (e) core thickness [t_{core}], (f) face sheets thickness [t_{face}], and (g) pore diameters (perforation ratios) [D_{pore}]

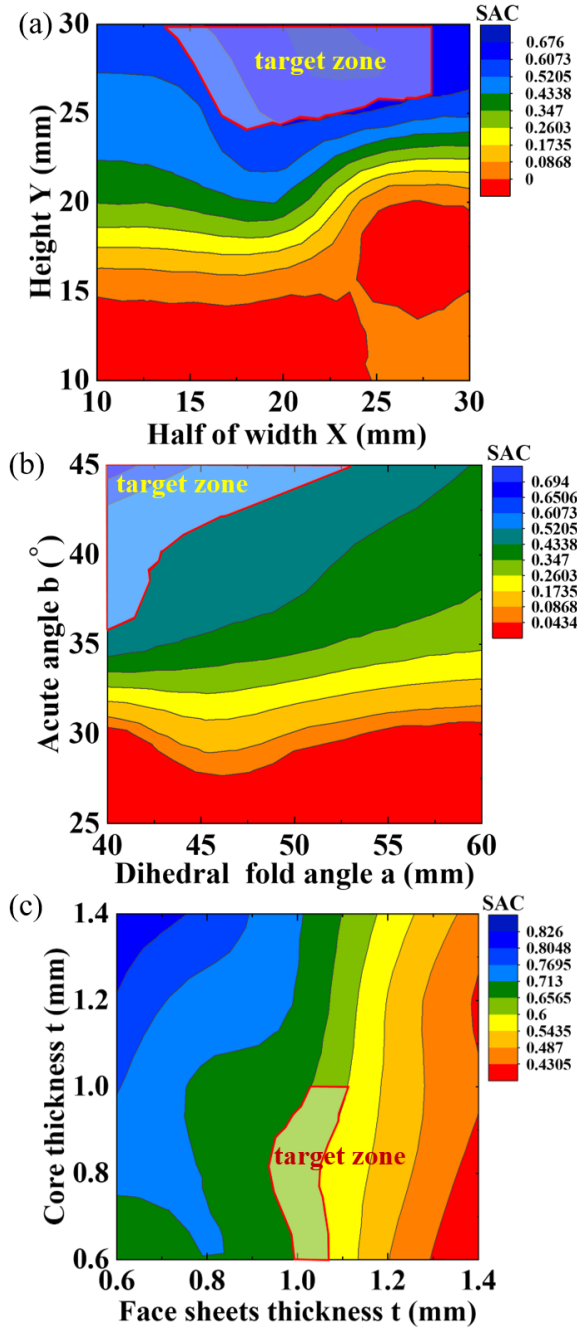


Figure. 9. Setup for the design target zone according to parameters

3.3 Fabrication

We fabricated a folded-core sandwich sound-absorbing structure using CF-PA thermoplastic polymer filaments as the base material and CCF filaments as the reinforcement material. Fig. 10(a) shows the types of materials used. To ensure optimal filament printing conditions, the height between the 3D printing nozzle and print bed was adjusted to an appropriate level during the bed level calibration. Two nozzles were used for the printing process: one for printing thermoplastic polymer filaments and the other for printing continuous fiber filaments. To optimize the 3D printing process, various variables such as the nozzle temperature, printing speed, bed temperature, and internal pattern filling were set using Aura, a 3D printing slicing software. Table 5 lists the values used for each variable during the printing process. During printing, the height between each nozzle and the print bed was adjusted to ensure proper adhesion and layer height.

Filaments with a diameter of 0.33 mm were extruded per layer onto the face sheet and core, with one layer of CCFs inserted into the face sheet. The face sheet was made of PA filaments dispersed with CCF and chopped carbon fibers, whereas the core was made of PA filaments dispersed with only chopped CFs for extrusion, as mentioned earlier.

The fabrication process for the folded-core sandwich structure is shown in Fig. 10(b). First, the core and face sheet were prepared by extrusion, where the core was $210 \times 100 \times 30$ mm and the face sheet was $210 \times 100 \times 1$ mm. Microperforations were then drilled into the face sheet using a trimming process, which produced holes with a diameter of 1 mm at a perforation rate of 1.32 %. The face sheet and core were then machined to have diameters of 98.8 mm and 28.8 mm, respectively, to measure the sound absorption performance using the impedance tube method. They were bonded with an adhesive film ((FM 73, Cytec, United States) and cured at 120 °C for 3 h to create sandwich structures. Finally, one sandwich structure was filled with soft PU foam and the other with GO-coated PU foam.

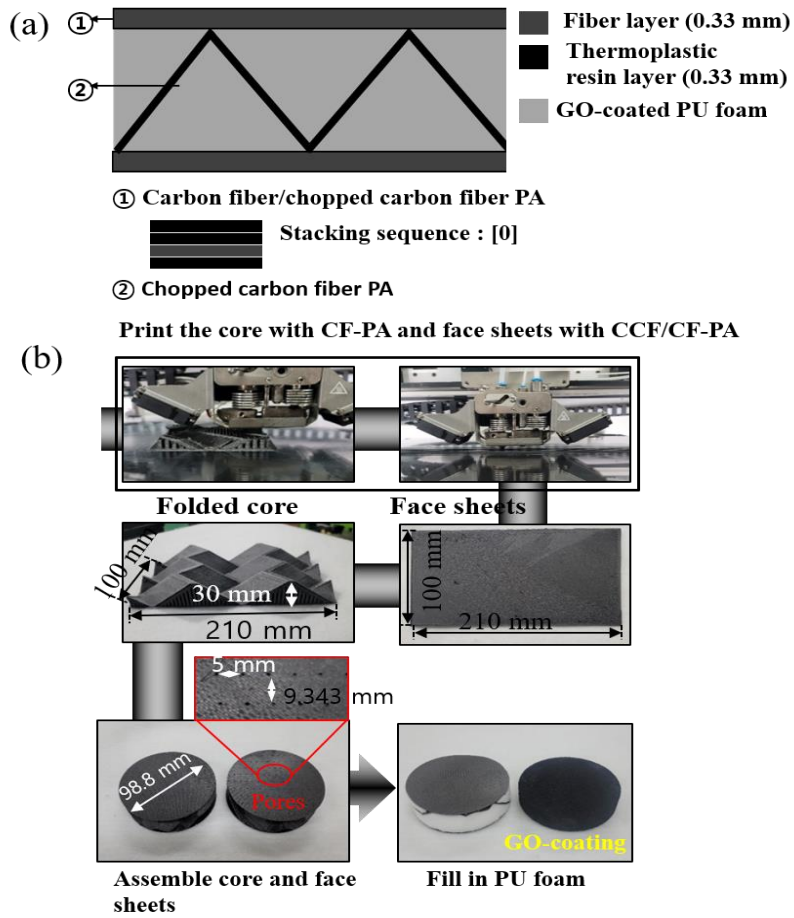


Figure. 10. The schematic of the folded core sandwich sound absorption structure and (b) the fabrication process of the 3D printed sound-absorbing folded core sandwich structure–filled GO–coated PU foam

Table 5

Summary of the parameters of the 3D printing parts.

Parameters	① CCF/CF-PA	② CF-PA
Nozzle temp [°C]	265	250
Bed temp [°C]	60	60
Fill pattern	Solid	Zigzag
Fill percentage	100	100
Single-layer thickness [mm]	0.33	0.33
Thickness [mm]	1	1

4. Results and discussion

4.1 Sound absorption performance

We prepared sound absorbing materials (soft PU foam and GO-coated PU foam) and measured their sound absorption performance before testing the folded-core sandwich SAS. We fabricated specimens to measure the sound absorption performance in the low-frequency band (160–1600 Hz) and the high-frequency band (1600–6000 Hz), because the specimen size varied depending on the frequency band. The equipment used and the specimens for the impedance tube measurement method are shown in Fig. 11(a). The measurement frequency range was set at 160–6000 Hz, covering the low-frequency band, because this range is relevant to the human audio frequency band (20–20000 Hz) and the frequency band in which humans are sensitive to sound (1000–5000 Hz). Fig. 11(b) shows the measured sound absorption performance of the soft and GO-coated PU foams. The sound-absorbing performances of both the generic and GO-coated PU foams were excellent, with a maximum of SAC 99 % or more in the mid- and high-frequency bands. However, the sound-absorbing performance of the GO-coated PU foam was relatively high in the low-frequency band (0–2400 Hz). This is because the flake-shaped GO forms a hierarchical structure that effectively absorbs sound waves in the low-frequency band. When sound waves arrive, the air spaces between the PU foam and GO vibrate microscopically, converting sound wave energy into heat energy. This mechanism is particularly effective at longer wavelengths, which are prevalent in the low-frequency bands. This is because sound waves in the high-frequency band have a shorter wavelength, and the air gaps between the PU foam and GO are too small to vibrate microscopically, resulting in less conversion of sound wave energy to heat energy⁽²⁰⁾. Therefore, the generic PU foam without GO coating performed better in the high-frequency band. When sound waves are incident on the internal path (tortuosity) of the PU foam, the air gaps between the GO particles prevent the microscopic vibration of the sound waves, similar to how the straightness of the sound wave prevents its dissipation. In the high-frequency band, the porous PU foam absorbs more sound wave energy, resulting in excellent absorption of sound energy^(8–11, 16, 21–23, 30).

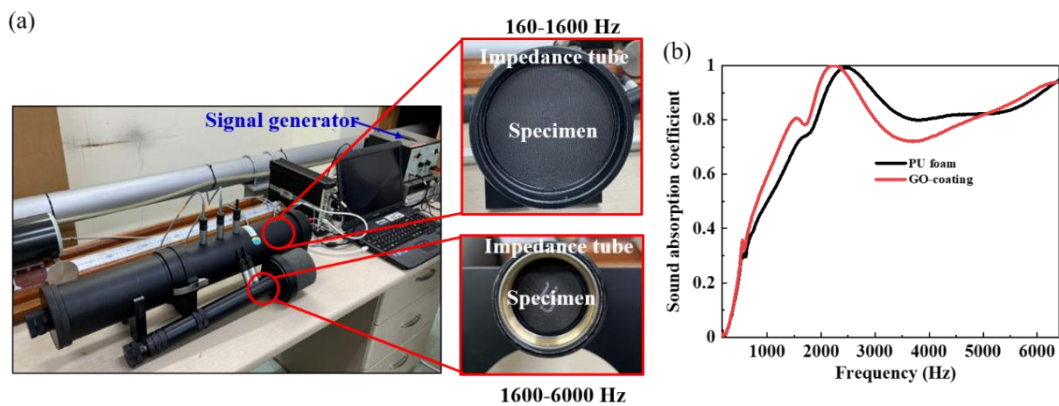


Figure. 11. The (a) sound absorption performance measurement system setup and specimens and (b) sound absorption coefficient of PU foam and GO-coated PU foam

Fig. 12(a) illustrates the SAC of a folded-core sandwich composite with both microperforated and non-microperforated face sheets analyzed by the finite difference and impedance tube methods in the low-frequency band (160–1600 Hz). In the numerical analysis, the structure with a non-microperforated face sheet showed a maximum SAC of 67 % at 630 Hz. In contrast, the structure with a microperforated face sheet showed a maximum SAC of 99 % at 1250 Hz. In contrast to the results of the numerical analysis, the impedance tube method showed a maximum SAC of 99 % at 606 Hz and 732 GHz for the structures with a non-microperforated face sheet and with a microperforated face sheet, respectively. In the numerical analysis, the non-microperforated structure

showed an SAC of 67%, but the measured SAC was as high as 99%. In addition, the numerical analysis showed that the microperforated structure had an SAC of 99% at 1250 Hz, but the measured SAC was 63% at 1250 Hz and 99% at 732 Hz. The difference between the numerical analysis and the measured results (obtained by the impedance tube method) could be due to the limited manufacturability in 3D printing and errors in the damping factor of the material. Moreover, the microperforated structure in the SAC exhibits a peak in a higher frequency band than the non-microperforated structure. As mentioned earlier, this is likely due to the increased resonant frequency caused by the larger air-hole interface area resulting from the microperforations when the sound waves are incident.

As the frequency band increased, the microperforated structure appeared to show better sound absorption performance. Fig. 12(b) illustrates the sound absorption performance of the folded core sandwich structure with and without microperforations filled with either soft PU foam or GO-coated PU foam. Both the soft PU foam and GO-coated PU foam fillings exhibited higher SAC peak values in the microperforated face sheet structure than in the non-microperforated face sheet structure. This is attributed to the increased air-hole interface area resulting from the microperforation, as mentioned earlier. Among the microperforated structures, the sandwich structure filled with GO-coated PU foam showed better sound absorption performance in the mid- and high-frequency bands (1800–6000 Hz) compared to the sandwich structure filled with general PU foam, except for the 1000–1800 Hz band. Comparing the sound absorption performance of the general PU foam and GO-coated PU foam alone, the former exhibited superior sound absorption performance in the high frequency band due to the straightness of the sound waves and the short wavelength. However, when the GO-coated PU foam was filled into the sandwich structure, it showed better sound absorption performance than the uncoated PU foam. This is because more sound waves were dissipated at the air gap interface of the GO-coated PU foam, and converted them into thermal energy.

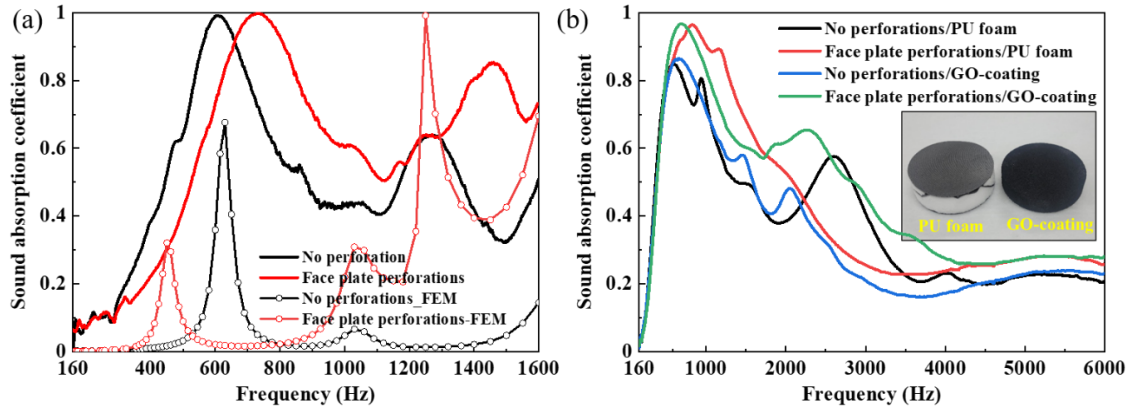


Figure. 12. Specimens for sound absorption measurements: (a) comparison between the sound absorption coefficient obtained by finite element (FE) simulation and the experimental no/face perforations folded core sandwich structure, (b) comparison of the sound absorption coefficient of the folded sandwich structure with different perforation configurations and GO coating

4.2 Mechanical test

A flatwise compression test was performed at the structural level to evaluate the mechanical performance of the fabricated folded-core sandwich sound-absorbing structure, as shown in Fig. 13(a). The test was performed in accordance with the ASTM C 365 standard using Instron 5582 equipment with a crosshead displacement speed of 0.5 mm per min. Fig. 13(b) shows a comparison of the compressive load of the folded-core sandwich structure proposed in this study with 3D printed sandwich structures that used thermoplastic polymer filaments and ceramic

materials presented in previous studies^(3, 4, 40~45, 50). The folded-core sandwich structure in this study showed a higher compressive load than other 3D printed sandwich structures^(35, 36). The compressive load in the presence or absence of microperforations on the face sheet was 811 N and 830 N, respectively, indicating that there was no significant difference. Thus, the microperforations had no significant effect on the compressive properties of the folded-core sandwich structure. In addition, the folded core sandwich structure filled with either soft foam or GO-coated PU foam exhibited a 24 % to 32 % higher compressive load capacity than the pristine specimens. This can be attributed to the load being distributed evenly across the foam, resulting in superior performance. This difference can be attributed to the hierarchical structures of the GO and PU foams, which improved the load-bearing properties of the interface.

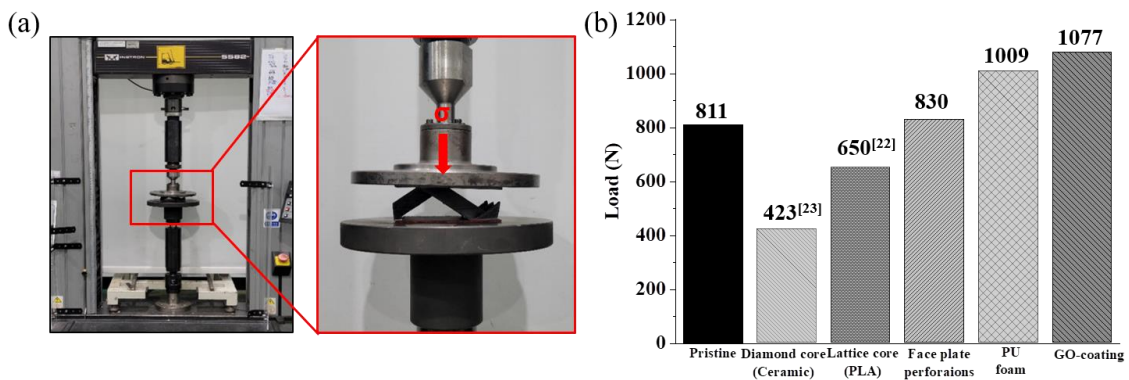


Figure. 13. The (a) setup for the flatwise compression test, performed according to ASTM C 365, and the (b) results of the flatwise compression test for the CCF-carbon fiber-dispersed polyamide (CF-PA), PU foam, and GO-coated folded structure composites

5. Conclusions

We have developed a novel 3D-printed sandwich SAS with microperforations filled with porous sound-absorbing materials. This folded-core structure was fabricated using a dual-nozzle FDM-type 3D printer, combining a CF-PA and CCF filaments. The Young's modulus, Poisson's ratio, and density of the resulting CCF/CF-PA composite structures were measured to develop a sandwich SAS that provides optimal low-frequency acoustic performance. Based on the measured physical properties, a sandwich SAS was designed to provide outstanding acoustic performance at low frequencies (160–1600 Hz) by optimizing the design parameters. Based on this design, the structure was fabricated using CF-PA as the folded core material.

CCF-CF-PA is the face sheet of the sandwich structure. To improve the sound absorption performance of the fabricated folded-core sandwich structure, efforts were made to improve the performance in the mid- and high-frequency bands (1600–6000 Hz). This was achieved by introducing a porous material, GO-coated PU foam. When comparing the sound absorption performance of the fabricated folded-core sandwich structure with and without microperforations, the first structure showed a peak sound absorption coefficient (SAC) in the higher-frequency band. Similar results were obtained for the structure filled with PU foam, where the structure filled with GO-coated PU foam showed better sound absorption performance than the structure filled with general soft PU foam. This is probably due to the air gap vibration between the interfaces, which leads to better sound absorption performance. The results of the compression test showed that there was no significant difference in strength between the microperforated and non-microperforated face sheets. When the sandwich structure was filled with a porous

material, the load was effectively distributed to the porous material, which increased the compressive load compared to a general folded-core sandwich structure. The hierarchical structure formed by GO enhanced the load-bearing effect and resulted in the largest compressive load. This demonstrates the exceptional durability of the structure and makes it an effective long-term solution for industrial, commercial, and residential noise mitigation.

Reference

- [1] Li T-T, Zhang. X, Wang H, Dai. W, Huang S-Y, Shiu. B-C, Lou. C-W, Lin J-H, "Sound absorption and compressive property of PU foam-filled composite sandwiches," Effects of needle-punched fabric structure, porous structure, and fabric-foam interface. *Polym Adv Technol*, vol. 31, no. 3, pp. 451-460, 2020.
- [2] Wang X, You F, Zhang F-S, Li J, Guo. S, "Experimental and theoretic studies on sound transmission loss of laminated mica-filled poly(vinyl chloride) composites," *J Appl Polym Sci*, vol. 122, no. 2, pp. 1427-1433, 2011.
- [3] Park CH, Kim DH, Moon YJ, "Computational study on the steady loading noise of drone propellers: Noise source modeling with the lattice Boltzmann method," *Int J Aeronaut Space Sci*, vol. 20, no. 4, pp. 858-869, 2019.
- [4] Wang Z, Huang J, Yi M, "Noise phase characteristics and the noise cancellation of twin-coaxial rotor based on phase modulation method," *Int J Aeronaut Space Sci*, vol. 23, pp. 834-847, 2022.
- [5] Groby J-P, Pommier R, Auregan Y, "Use of slow sound to design perfect and broadband passive sound-absorbing materials," *Acoust Soc Am*, vol. 139, no. 4, pp.1660-1671, 2016.
- [6] Chen C, Du Z, Hu G, Yang. J, "A low-frequency sound-absorbing material with subwavelength thickness," *Appl Phys Lett*, vol. 110, no. 22, 221903, 2017.
- [7] Verdejo R, Stämpfli R, Alvarez-Lainez M, Mourad S, Rodriguez-Perez MA, Brühwiler PA, Shaffer M, "Enhanced acoustic damping in flexible PU foams filled with carbon nanotubes," *Compos Sci Technol*, vol. 69, no. 10, pp. 1564-1569, 2009.
- [8] Jiang X, Wang Z, Yang Z, Zhang F, You F, Yao C, "Preparation and sound absorption properties of barium titanate/nitrile butadiene rubber-PU foam composites with stratified structure," *RSC Adv*, vol. 8, pp. 20968-20975, 2018.
- [9] Bahrambeygi H, Sabetzadeh N, Rabbi A, Nasouri K, Shoushtari AM, Babaei MR, "Nanofibers (PU and PAN) and nanoparticles (Nanoclay and MWNTs) simultaneous effects on PU foam sound absorption," *J Polym Res*, vol. 20, no. 72, 2013.
- [10] Bardakhanov SP, Lee C-M, Goverdovskiy VN, Zavjalov AP, Zobov KV, Chen M, Xu ZH, Chakin IK, Trufanov DY, "Hybrid sound-absorbing foam materials with nanostructured grit-impregnated pores," *Appl Acoust*, vol. 139, pp. 49-74, 2018.
- [11] Kim JM, Kim DH, Kim J, Lee JW, Kim WN, "Effect of graphene on the sound damping properties of flexible PU foams," *Macromol Res*, vol. 25, pp. 190-196, 2017.
- [12] Xie S, Yang S, Yang C, Wan. D, "Sound absorption performance of a filled honeycomb composite structure," *Appl Acoust*, vol. 162, 107202, 2020.
- [13] Wang D-W, Ma. L, "Sound transmission through a composite sandwich plate with pyramidal truss cores," *Compos Struct*, vol. 164, pp. 104-117, 2017.
- [14] Shengchun W, Zhaoxiang D, Weidong. S, "Sound transmission loss characteristics of unbounded orthotropic

- sandwich panels in bending vibration considering transverse shear deformation,” *Compos Struct*, vol. 92, no. 12, pp. 2885–2889, 2010.
- [15] Song Y, Feng L, Wen J, Yu D, Wen X, “Reduction of the sound transmission of a periodic sandwich plate using the stop band concept,” *Compos Struct*, vol. 128, pp. 428–436, 2015.
- [16] Yang M, Sheng P, “Sound absorption structures: From porous media to acoustic metamaterials.” *Annu Rev Mater Sci*, vol. 47, no. 1, pp. 83–114, 2017.
- [17] Wang T, Li S, Rajaram S, Nutt SR, “Predicting the sound transmission loss of sandwich panels by statistical energy analysis approach,” *J Vib Acoust*, vol. 132, no. 1, 011004, pp. 1–7, 2010.
- [18] Xin FX, Lu TJ, Chen CQ, “Sound transmission through simply supported finite double-panel partitions with enclosed air cavities,” *J Vib Acoust*, vol. 132, no. 1, 011008, pp. 1–11, 2010.
- [19] Price AJ, Crocker MJ, “Sound transmission through double panels using statistical energy analysis,” *J Acoust Soc Am*, vol. 47, pp. 683–693, 1970.
- [20] Xie S, Wang D, Feng Z, Yang S, “Sound absorption performance of microperforated honeycomb metasurface panels with a combination of multiple orifice diameters,” *Appl Acoust*, vol. 158, 107046, 2020.
- [21] Shen C, Xin FX, Lu TJ, “Theoretical model for sound transmission through finite sandwich structures with corrugated core,” *Int J Non Linear Mech*, vol. 47, no. 10, pp. 1066–1072, 2012.
- [22] Yang C, Cheng L, “Sound absorption of microperforated panels inside compact acoustic enclosures,” *J Sound Vib*, vol. 360, pp. 140–155, 2016.
- [23] Lin J–H, Lin C–M, Huang C–C, Lin C–C, Hsieh C–T, Liao Y–C, “Evaluation of the manufacture of sound absorbent sandwich plank made of PET/TPU honeycomb grid/PU foam,” *J Compos Mater*, vol. 45, no. 13, pp. 1355–1362, 2011.
- [24] Ning F, Cong W, Qiu J, Wei J, Wang S, “Additive manufacturing of carbon fiber reinforced thermoplastic composites using fused deposition modeling,” *Compos B: Eng*, vol. 80, pp. 369–378, 2015.
- [25] Mazzanti V, Malagutti L, Mollica, “FDM 3D printing of polymers containing natural fillers: A review of their mechanical properties,” *Polymers*, vol. 11, no. 7, 1094, 2019.
- [26] Korede JM, Shaikh M, Kandasubramania. B, “Bionic prototyping of honeycomb patterned polymer composite and its engineering application,” *Polym Plast Technol Eng*, vol. 57, no. 17, pp. 1828–1844, 2108.
- [27] Park SJ, Park JH, Lee KH, Lyu MY, “Deposition strength of specimens manufactured using fused deposition modeling type 3D printer,” *Polymer (Korea)*, vol. 40, no. 6, pp. 846–851, 2016.
- [28] Sugiyama K, Matsuzaki R, Ueda M, Todoroki A, Hirano Y, “3D printing of composite sandwich structures using continuous carbon fiber and fiber tension,” *Compos Part A Appl Sci Manufact*, vol. 113, pp. 114–121, 2018.
- [29] Surange VG, Gharat PV, “3D printing process using fused deposition modelling (FDM),” *Int Res J Eng Technol*, vol. 3, no. 3, pp. 1403–1406, 2016.
- [30] Ngo TD, Kashani A, Imbalzano G, Nguyen KTQ, Hui D, “Additive manufacturing (3D printing): A review of materials, methods, applications and challenges,” *Compos B Eng*, vol. 143, pp. 172–196, 2018.
- [31] Wang X, Jiang M, Zhou Z, Gou J, Hui D, “3D printing of polymer matrix composites: A review and prospective,” *Compos B: Eng*, vol. 110, pp. 442–458, 2017.

- [32] Ivanova O, Williams C, Campbell T, "Additive manufacturing (AM) and nanotechnology: Promises and challenges," *Rapid Prototyp J*, vol. 19, no. 5, pp. 353–364, 2013.
- [33] Gu DD, Meiners W, Wissenbach K, Poprawe R, "Laser additive manufacturing of metallic components: Materials, processes and mechanisms," *Int Mater Rev*, vol. 57, no. 3, pp. 133–164, 2012.
- [34] Wei X, Li D, Jiang W, Gu Z, Wang X, Zhang Z, Sun Z, "3D printable graphene composite," *Sci Rep*, vol. 5, 11181, 2015.
- [35] Al Abadi H, Thai H-T, Paton-Cole V, Patel VI, "Elastic properties of 3D printed fibre-reinforced structures," *Compos Struct*, vol. 193, pp. 8–18, 2018.
- [36] Vinoth Babu N, Venkateshwaran N, Rajini N, Ismail SO, Mohammad F, Al-Lohedan HA, Suchart S, "Influence of slicing parameters on surface quality and mechanical properties of 3D-printed CF/PLA composites fabricated by FDM technique," *Mater Technol*, vol. 37, no. 9, pp. 1008–1025, 2022.
- [37] Baumann F, Scholz J, Fleischer J, "Investigation of a new approach for additively manufactured continuous fiber-reinforced polymers," *Procedia CIRP*, vol. 66, pp. 323–328, 2017.
- [38] Chacón JM, Caminero MA, Núñez PJ, García-Plaza E, García-Moreno I, Reverte JM, "Additive manufacturing of continuous fibre reinforced thermoplastic composites using fused deposition modelling: Effect of process parameters on mechanical properties," *Compos Sci Technol*, vol. 181, 107688, 2019.
- [39] Chaudhry FN, Butt SI, Mubashar A, Naveed AB, Imran SH, Faping Z, "Effect of carbon fibre on reinforcement of thermoplastics using FDM and RSM," *J Thermoplast Compos Mater*, vol. 35, no.3, pp. 352–374, 2022.
- [40] Melenka GW, Cheung BKO, Schofield JS, Dawson MR, Carey JP, "Evaluation and prediction of the tensile properties of continuous fiber-reinforced 3D printed structures," *Compos Struct*, vol. 153, pp. 866–875, 2016.
- [41] Wu Q, Ma L, Wu L, Xiong J, "A novel strengthening method for carbon fiber composite lattice truss structures," *Compos Struct*, vol. 153, pp. 585–592, 2016.
- [42] Wang Z, Luan C, Liao G, Yao X, Fu J, "Mechanical and self-monitoring behaviors of 3D printing smart continuous carbon fiber-thermoplastic lattice truss sandwich structure," *Compos B Eng*, vol. 176, 107215, 2019.
- [43] Mori K-I, Maeno T, Nakagawa Y, "Dieless forming of carbon fibre reinforced plastic parts using 3D printer," *Procedia Eng*, vol. 81, pp. 1595–1600, 2014.
- [44] Dudek P, "FDM 3D printing technology in manufacturing composite elements," *Arch Metall Mater*, vol. 58, no. 4, pp. 1415–1418, 2013.
- [45] Nguyen NA, Bowland CC, Naskar AK, "A general method to improve 3D-printability and inter-layer adhesion in lignin-based composites," *Appl Mater Today*, vol.12, pp. 138–152, 2018.
- [46] Nannan G, Leu MC, "Additive manufacturing: technology, applications and research needs." *Front Mech Eng*, vol. 8, pp. 215–243, 2013.
- [47] Quan Z, Wu A, Keefe M, Qin X, Yu J, Suhr J, Byun J-H, Kim B-S, Chou T-W, "Additive manufacturing of multidirectional preforms for composites: opportunities and challenges," *Mater Today*, vol. 18, no. 9, pp. 503–512, 2015.
- [48] Gianni S, Di Nisio A, Lanzolla AM, Ragolia M, Percoco G, "Fused filament fabrication of commercial conductive filaments: Experimental study on the process parameters aimed at the minimization, repeatability

- and thermal characterization of electrical resistance,” *Int J Adv Manuf Technol*, vol. 111, no. 9–10, pp. 2971–2986, 2020.
- [49] Singamneni S, LV Yifan, Hewitt. A, Chalk R, Thomas W, Jordison D, “Additive manufacturing for the aircraft industry: A review,” *J Aeronaut Aerosp Eng*, vol. 8, pp. 0–13, 2019.
- [50] Kim J, Shin D, Jang S, Kim T, Kim G–H, Jung K, Kim HG, Park JH, “Applicability of the Ti6Al4V alloy to the roller arm for aircraft parts made using the DMLS method,” *Int J Aeronaut Space Sci*, vol. 23, no. 5, pp. 896–905, 2022.
- [51] Meng H, Galland MA, Ichchou M, Bareille O, Xin FX, Lu TJ, “Small perforations in corrugated sandwich panel significantly enhance low–frequency sound absorption and transmission loss,” *Compos Struct*, vol. 182, pp. 1–11, 2017.
- [52] Quan C, Bin H, Hou Z, Zhang Q, Tian X, Lu TJ, “3D printed continuous fiber reinforced composite auxetic honeycomb structures,” *Compos B Eng*, vol. 187, 107858, 2020.
- [53] Akiwate DC, Date MD, Venkatesham B, Suryakumar S, “Acoustic characterization of additive manufactured perforated panel backed by honeycomb structure with circular and non–circular perforations,” *Appl Acoust*, vol. 155, pp. 271–279, 2019.
- [54] Oh J–H, Kim J–S, Nguyen VH, Oh I–K, “Auxetic graphene oxide–porous foam for acoustic wave and shock energy dissipation,” *Compos B Eng*, vol. 18, 107817, 2020.
- [55] Wang D–W, Wen Z–H, Glorieux C, Ma L, “Sound absorption of face–centered cubic sandwich structure with micro–perforations,” *Mater Des*, vol. 186, 108344, 2020.
- [56] Liu Z, Zhan J, Fard M, Davy JL, “Acoustic properties of multilayer sound absorbers with a 3D printed micro–perforated panel,” *Appl Acoust*, vol. 121, pp. 25–32, 2017.
- [57] Azzouz L, Chen Y, Zarrelli M, Pearce JM, Mitchell L, Ren Grasso M, “Mechanical properties of 3–D printed truss–like lattice biopolymer nonstochastic structures for sandwich panels with natural fibre composite skins,” *Compos Struct*, vol. 213, pp. 220–230, 2019.
- [58] Ghannadpour SAM, Mahmoudi M, Hossein NK, “Structural behavior of 3D–printed sandwich beams with strut–based lattice core: Experimental and numerical study,” *Compos Struct*, vol. 281, 115113, 2022.
- [59] Photiou D, Avraam S, Sillani F, Verga F, Jay O, Papadakis L, “Experimental and numerical analysis of 3D printed polymer tetra–petal auxetic structures under compression,” *Appl Sci*, vol. 11, no. 21, 10362, 2021.
- [60] Tabacu S, Ducu C, “Numerical investigations of 3D printed structures under compressive loads using damage and fracture criterion: Experiments, parameter identification, and validation,” *Extreme Mech Lett*, vol. 39, 100775, 2020.
- [61] van de Werken N, Tekinalp H, Khanbolouki P, Ozcan S, Williams A, Tehrani M, “Additively manufactured carbon fiber–reinforced composites: State of the art and perspective,” *Addit Manuf*, vol. 31, 100962, 2020.
- [62] Santos JD, Fernández A, Ripoll L, Blanco N, “Experimental characterization and analysis of the in–plane elastic properties and interlaminar fracture toughness of a 3D–printed continuous carbon fiber–reinforced composite,” *Polymers*, vol. 14, no. 3, pp. 506, 2022.